JREE: Vol. 9, No. 3, (Summer 2022) 32-44

Journal of Renewable Energy and Environment

Journal Homepage: www.jree.ir

Materials and Energy Research Center

MERC

Research Article

DC Microgrid Voltage Stability through Inertia Enhancement Using a Bidirectional DC-DC Converter

Shokoofeh Bagheri [a], Hassan Moradi CheshmehBeigi [a,b*]

[a] *Department of Electrical Engineering, Faculty of Engineering, Razi University, P. O. Box: 67144-14971, Kermanshah, Iran.*
[b] *Industrial Intelligent Systems Research Center (IISRC), Razi University, Kermanshah, Iran.*

PAPER INFO

Paper history:
Received: 01 October 2021
Revised in revised form: 27 December 2021
Scientific Accepted: 12 December 2021
Published: 28 May 2022

Keywords:
Renewable Energy Source (RES),
DC Microgrid (DCMG),
Cascaded Buck-Boost Converter (CBBC),
Virtual Inertia,
Virtual DC Machine (VDCM),
DC Bus

ABSTRACT

Today, the presence of energy storage systems along with the alternative nature of renewable energy sources has become undeniable and one of these types of systems is battery energy storage systems. The most important factor in studying the stability of DC microgrids (DCMGs) is the stabilization of the DC bus voltage when an error occurs on its reference value. Therefore, batteries along with power electronic converters play an important role in maintaining DCMG stability. In this paper, the use of Cascaded Buck-Boost Converter (CBBC) can be considered as a suitable alternative to bidirectional buck-boost converter due to such advantages as high power density, 98 % efficiency, and higher operating temperature in battery. The control strategy is applied in the microgrid implemented in the converter system set with storage, and Virtual DC Machine (VDCM) is based on charging and discharging battery through CBBC. In the studied control method, the theoretical properties of the DC machine, which is responsible for amplifying the virtual inertia in the system, are directed to the CBBC for correct switching. VDCM can be changed from motoring to generating mode or vice versa, regardless of mechanical machinery. Therefore, the proposed control system is simulated in an islanded DCMG in Matlab/Simulink and the stability of the studied system is analyzed according to the small-signal model of the proposed control and converter units. According to the simulation results and small-signal model analysis, the stability of the proposed idea under different scenarios is confirmed.

https://doi.org/10.30501/jree.2021.298032.1233

1. INTRODUCTION

The development of industry in the 21st century compared to the 18th century has caused many gaps in electricity consumption to the extent that this has led to global energy supply problems. Given the declining trend in fossil fuel resources, now is the time to take fundamental steps to address this major challenge. Also, due to the difficult conditions for the transportation of conventional energy resources to remote areas that do not have access to the route of large power plants and their electricity must be provided autonomously [1]; today, the share of power generation for these areas is associated with the high penetration of Renewable Energy Sources (RESs) [2]. However, on the other hand, all RESs have unique performance characteristics and to integrate them simultaneously, it is necessary to create a suitable method for the optimal use of these resources in the system. For example, one of these features is the random and alternating nature of renewable energy output, which will have a significant impact on system power quality, voltage, and frequency. Therefore, to solve this problem, energy storage technology was provided in the system [3]. In fact, energy storage points to a significant improvement in the efficiency, stability, and resilience of the power grid [4]. On the other hand, due to the remoteness of some areas from the utility grid and the location of sources that have units with DC output including photovoltaic (PV) systems, Fuel Cell (FC), Energy Storage System (ESS), and DC loads, and this has led to the wider applicability of DC microgrids (DCMGs) [5]. The most important factor studied to analyze the stability of DCMGs is to adjust the DC bus voltage to its reference value. Factors that cause instability when faults occur in DCMGs are fluctuations in the output power of RESs and frequent switching of AC or DC loads with different power consumption. Therefore, to improve the quality of DCMG performance, the implementation of virtual inertia control technique through battery energy storage system and Power Electronic Converters (PECs) has been proposed. Virtual inertia mimicry that results from simulation of the mechanical inertia properties of a rotating machine, i.e., synchronous generators (SGs) in the power grid, is essential to describing the dynamic behavior and stability of the grid [6]. The first concept is the proposed control technique of virtual synchronous generators [7, 8]. In [9], virtual inertia was developed according to the dynamic behavior of the battery based on the second-order SG model with the MUltiple signal

*Corresponding Author's Email: ha.moradi@razi.ac.ir (H. Moradi CheshmehBeigi)
URL: https://www.jree.ir/article_150510.html

Please cite this article as: Bagheri, Sh. and Moradi CheshmehBeigi, H., "DC microgrid voltage stability through inertia enhancement using a bidirectional DC-DC converter", ***Journal of Renewable Energy and Environment (JREE)***, Vol. 9, No. 3, (2022), 32-44. (https://doi.org/10.30501/jree.2021.298032.1233).

2423-7469/© 2022 The Author(s). Published by MERC. This is an open access article under the CC BY license (https://creativecommons.org/licenses/by/4.0/).

classification (MUSIC) algorithm technique. To mimic virtual inertia in low-voltage islanded DCMGs, the coordinated control based on bus signaling was investigated in [10]. The authors in [11] proposed adaptive virtual inertia control based on the variable droop coefficient. In this method, by changing the DC bus voltage, the droop characteristic actually changes, that is, the voltage change rate is defined as a variable of the droop coefficient function. Continuous virtual inertia with predictive control, improved active damping compensation, and the use of additional ESSs in [12-14] were studied to maintain DC bus voltage stability and reduce the effect of constant power load. Negative damping of the DC converter immediately creates a positive feedback that causes instability in the DC link voltage; thus, a virtual inertia technique is proposed by forming a negative feedback loop to improve the damping performance and stability of the DC voltage in [15]. In order to create DCMG stability, damping amplification was proposed by implementing the frequency-dependent virtual impedance method when using RESs in [16]. In [17-19], the transient response process of the power system was enhanced with the help of virtual inertia control and virtual capacitor, but the stability analysis of controlling the increase in damping of DC link voltage fluctuations and inertia was omitted. In [20], the aim was to implement an inertia and damping control strategy based on charging and discharging capacitors using ESS. This technique was used to control the output parameters of DCMG converters. Other implemented virtual inertia simulation methods included droop + low pass filter control and power management technique based on charging and discharging the battery energy storage system based on DCMG power flow in [21, 22]. Despite the implementation of all the introduced control techniques, the introduction of a Virtual DC Machine (VDCM) scheme for virtual inertia simulation has recently been welcomed [23] and the aim of this paper is to improve the VDCM design using accurate real DC machine equations. Using the mechanical equations governing the rotor of a real DC machine, the inertia properties can be applied to a bidirectional DC-DC converter. In order to maintain stability and control DC bus voltage disturbances, the connection between the ESS converter and the bus is designed to be flexible. On the other hand, choosing the Cascaded Buck-Boost Converter (CBBC) can be very effective in the performance of the VDCM unit. The proposed converter is considered due to the ability to reverse the working direction and transfer enough power when needed for different modes of operation [24, 25]. The objectives of the article are:

- The problem of inertia deficiency can be solved with the presence of battery by presenting virtual inertia emulation based on real DC machine equations and CBBC;
- Flexible exchange of VDCM power flow on initial transient response and fault moments in DCMG;
- Optimal battery performance using correct CBBC switching for charging and discharging mode;
- Reducing DC bus voltage drop significantly compared to conventional scheme;
- Checking the performance of the CBBC as an interface between battery and DCMG;
- Evaluation of system stability using the small-signal model of the proposed VDCM control scheme and CBBC;
- Simulation of the proposed scheme in an islanded DCMG (see Figure 1(a)) under different scenarios and comparison with the typical scheme;

This article is organized as follows: The structure of an islanded DCMG is introduced in Section 2. The concept of virtual inertia, VDCM modeling, and control strategy are presented in Section 3. Section 4 examines the VDCM stability analysis with small-signal modeling. Finally, the validation of the simulation results and the final conclusion are presented in Sections 5 and 6, respectively.

2. PROPOSED STRUCTURE OF THE STUDIED DCMG

The structure of the DCMG studied including Wind Turbine (WT), PV module, FC stack, battery, and local AC and DC loads is shown in Figure 1(a), 1(b). Each unit is connected to the DC bus in parallel via PECs. However, it is difficult to maintain the bus voltage due to the different nature of the mentioned units under momentary changes in sources and loads. DCMG can be described in three parts: 1) RESs production unit: WT based on the Permanent Magnet Synchronous Generator (PMSG) and the PV that are connected to the bus via a DC-DC boost converter. However, to rectify the output current of the WT, the Gritz 3-phase diode bridge is used before the boost converter; 2) Backup unit: The FC connected to the boost converter and the lead-acid battery connected to the bidirectional CBBC are used to ensure power balance and continuity in microgrid stability; 3) Load unit: The AC and DC loads are connected to the DCMG via a Voltage Source Inverter (VSI) and buck converter, respectively. Since the main focus of this paper is on the concept of inertia amplification via VDCM in DCMG, the modeling and design of other component controllers in this paper has been omitted.

3. DETAILED DESCRIPTION OF THE PROPOSED CONTROLLER STRUCTURE

3.1. Principle of virtual inertia

SGs are usually power generators in conventional power grids. SGs are rotary machines that, due to their high inertia, prevent changes in grid frequency when a sudden error occurs. The concept of inertia means the inherent resistance to changing the angular velocity of a rotating object. On the other hand, although power generation with the help of RESs has significant advantages today, the use of this type of generators causes problems such as reducing inertia in the grid. Now, in order to improve the performance of the grid or microgrid, the virtual inertia emulation technique can be used in the system. The use of PECs along with the implementation of its proper control technique to perform the correct switching operation is one of the new methods that has recently been considered to emulate virtual inertia in the system, whose coordination between this processes proves the stability of the grid.

3.2. VDCM modeling

The battery with a single-phase converter connected to it and the implemented control system form the VDCM set, which will first introduce the CBBC converter in Figure 2(a). The use of 4 active switches in this converter caused the power transfer between two DC sources in two different directions. According to the figure, the proposed converter has 4

operating modes: charge, transfer, discharge, and idle. Under these conditions, the DC bus voltage can be adjusted to its reference value by the appropriate delivery d to the active switches. Therefore, using this converter to change the performance of the virtual machine in different operating modes of motoring, generating, and standby in the field of storage is a good option that motors operation to support the required power load using the battery power supply, the generating operation is to store additional DCMG power in the battery and standby operation occurs when there is a power balance between supply and demand in microgrid.

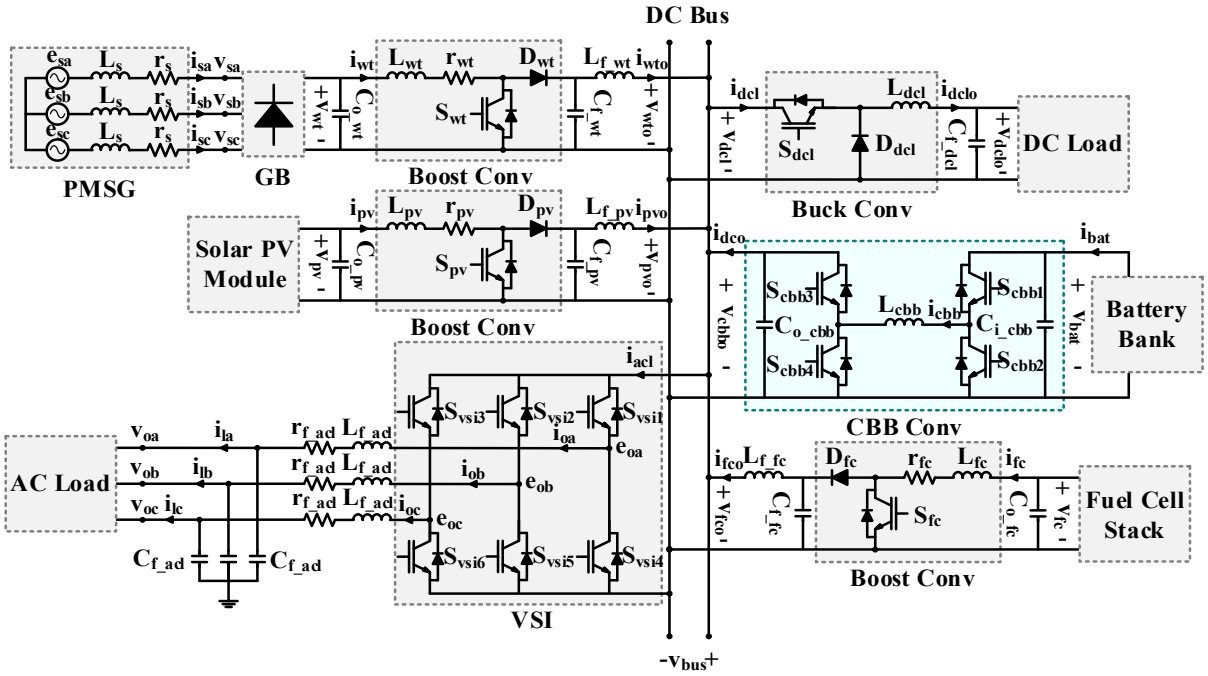

(a)

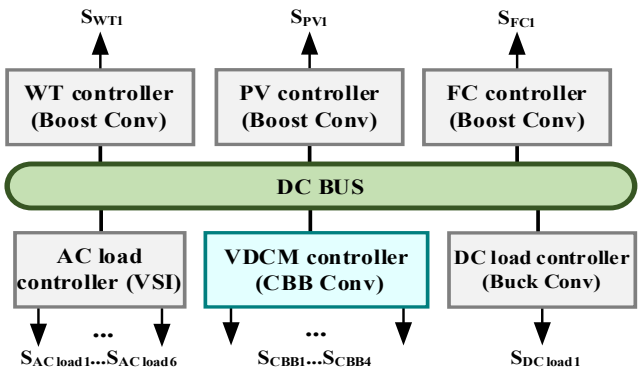

(b)

Figure 1. (a) Structure of the islanded DCMG; (b) Typical scheme of the DCMG controller

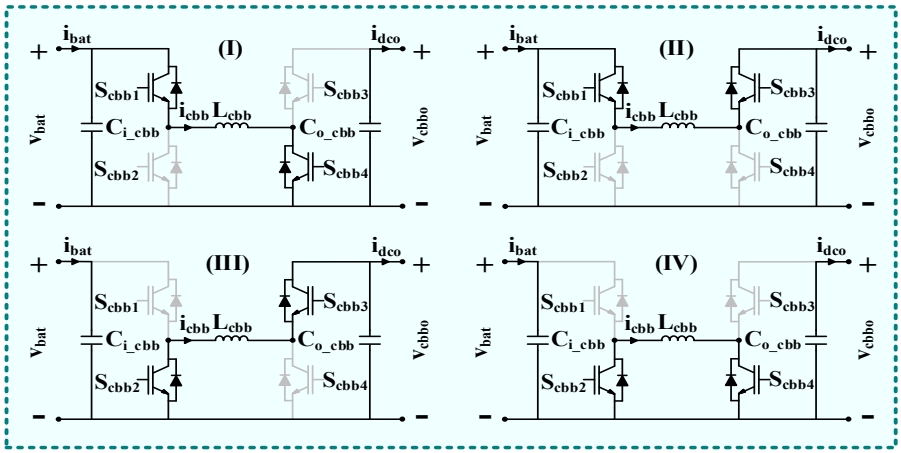

(a)

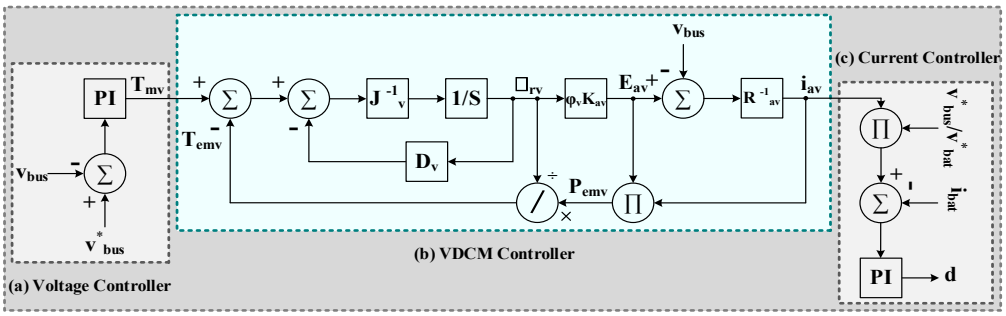

(b)

Figure 2. (a) Operating modes of the proposed converter (CBBC), (b) Controller of the virtual inertia part

3.3. Control strategy

One of the important purposes of inserting an output capacitor in a VDCM system is to improve the DC bus voltage transient in the event of a DCMG fault. By storing electrical energy (equivalent to inertia) in the output capacitor, active power support is provided to the system. In this way, Relations 1 and 2 can be considered equivalent to each other:

$$W_r = \frac{1}{2} J_v \omega_{rv}^2 \quad (1)$$

$$W_e = \frac{1}{2} C_{dc} v_{dc}^2 \quad (2)$$

According to Figure 2(b) the implemented control strategy based on a separately excited DC machine, which is in fact the control of bus voltage, is equivalent to controlling the speed of DC machine [26]. The virtual inertia control unit consists of 3 main blocks, i.e., DC bus voltage controllers, VDCM, current regulation and PWM modulation. In the bus voltage control unit, first, using the PI controller, based on the amount of difference between the bus voltage reference and its measured value at any moment, T_{mv} is obtained. This value is then entered into the VDCM controller unit and based on Equations 3-5, I_{av} is determined. In the next block, the purpose is to determine the appropriate d for the correct switching CBBC for the PWM block. In this section, I_{av} is multiplied by the conversion constant $\frac{V^*_{bus}}{V^*_{bat}}$ to get the I^*_{bat}. The value obtained is compared with the measured value. Finally, upon entering the PI controller, the converter is required in the operating mode.

$$T_{emv} - T_{mv} = J_v \frac{d\omega_{rv}}{dt} + D_v \omega_{rv} \quad (3)$$

$$P_{emv} = E_{av}\, I_{av}, T_{emv} = \frac{P_{emv}}{\omega_{rv}} \rightarrow P_{emv} = T_{emv}\, \omega_{rv} \quad (4)$$

$$V_{bus} - E_{av} = R_{av}\, I_{av} \quad (5)$$

Table 1. DCMG system parameters

VDCM system parameters						Other parameters	
Parameter	**Value**	**Parameter**	**Value**	**Parameter**	**Value**	**Parameter**	**Value**
V^*_{bat}	96 V	$\varphi_v K_{av}$	9.45015	V^*_{bus}	400 V	P^*_{DCMG}	18 KW
P^*_{VDCM}	4 KW	C_{i_cbb}	1 mF	Switches type	IGBT/Diode	P^*_{PMSG}	5 KW
R_{av}	1 Ω	C_{o_cbb}	2 mF	K^P_{VC}	50	P^*_{PV}	5 KW
J_v	0.001	L_{cbb}	50 µH	K^I_{VC}	1.5	P^*_{FC}	4 KW
D_v	0.5	SoC	80 %	K^P_{CC}	65	$P^*_{AC\ load}$	7 KW
L_v	0.5 mH	f_s	5 KHz	K^I_{CC}	8	$P^*_{DC\ load}$	4 KW

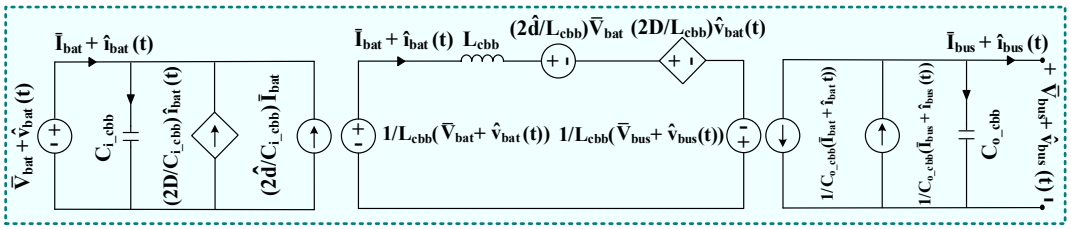

(a)

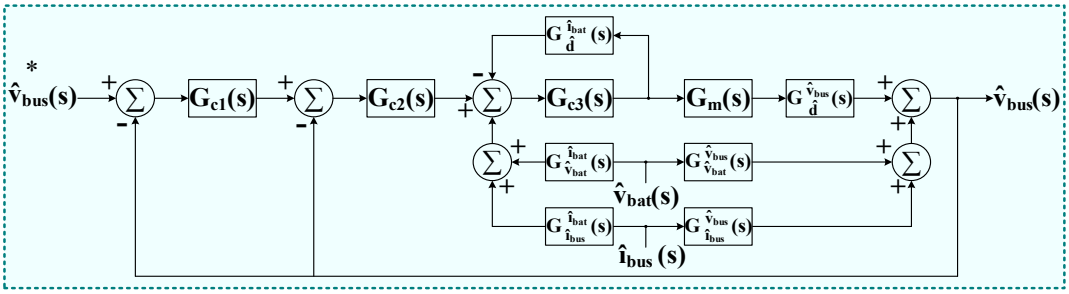

(b)

Figure 3. Small-signal model of the VDCM: (a) Small-signal model of the CBBC, (b) Block diagram model of the control VDCM system

4. STABILITY ANALYSIS OF THE VDCM SYSTEM

To evaluate the stability of VDCM implemented in DCMG in small disturbances, first, the CBBC small-signal model in Figures 3(a), 3(b) and the control system applied to it by system linearization are analyzed [27].

In this section, Equations 6 and 7 are first obtained using Figure 3(a) and relations KVL and KCL applied to the CBBC.

$$\frac{(1-C_{o\_cbb})}{C_{o\_cbb}}[\bar{I}_{bus}+\hat{i}_{bus}(t)]-\frac{1}{sC_{o\_cbb}L_{cbb}^{\ 2}}[\bar{V}_{bat}+\hat{v}_{bat}(t)]+\frac{2\hat{d}}{sC_{o\_cbb}L_{cbb}^{\ 2}}\bar{V}_{bat}+\frac{2D}{sC_{o\_cbb}L_{cbb}^{\ 2}}\hat{v}_{bat}(t)-\frac{1+(sC_{o\_cbb}L_{cbb})^2}{sC_{o\_cbb}L_{cbb}^{\ 2}}[\bar{V}_{bus}+\hat{v}_{bus}(t)]=0 \quad (6)$$

$$-\frac{1}{L_{cbb}}[\bar{V}_{bat}+\hat{v}_{bat}(t)]+\frac{1+(sC_{o\_cbb}L_{cbb})^2}{sC_{o\_cbb}^{\ 2}L_{cbb}}[\bar{I}_{bat}+\hat{i}_{bat}(t)]+\frac{2\hat{d}}{L_{cbb}}\bar{V}_{bat}+\frac{2D}{L_{cbb}}\hat{v}_{bat}(t)-\frac{(1-C_{o\_cbb})}{sC_{o\_cbb}^{\ 2}L_{cbb}}[\bar{I}_{bus}+\hat{i}_{bus}(t)]=0 \quad (7)$$

According to Figure 2(b) in the small-signal model, Relationships 8-12 are calculated:

$$\Delta V\left(K_{VC}^{P}+\frac{K_{VC}^{I}}{s}\right)=T_{mv} \quad (8)$$

$$T_{mv}-T_{emv}=\Delta T_v \quad (9)$$

$$(\Delta T_v-D_v\omega_{rv})\frac{1}{sJ_v}=\omega_{rv} \quad (10)$$

$$\omega_{rv}\varphi_v K_{av}=E_{av} \quad (11)$$

$$E_{av}\left(\frac{sJ_vR_{av}+D_vR_{av}+(\varphi_vK_{av})^2}{\varphi_vK_{av}R_{av}}\right)=\Delta V\left(\frac{sK_{VC}^{P}+K_{VC}^{I}}{s}\right) \quad (12)$$

and…:

$$G_{vv}(s)=\frac{\hat{v}_{bus}}{\hat{v}_{bat}}=\frac{2D-1}{1+(sC_{o\_cbb}L_{cbb})^2} \quad (13)$$

$$G_{vd}(s)=\frac{\hat{v}_{bus}}{\hat{d}}=\frac{2\bar{V}_{bat}}{1+(sC_{o\_cbb}L_{cbb})^2} \quad (14)$$

$$Z(s)=\frac{\hat{v}_{bus}}{\hat{i}_{bus}}=\frac{s(1-C_{o\_cbb})L_{cbb}^{\ 2}}{1+(sC_{o\_cbb}L_{cbb})^2} \quad (15)$$

$$G_{iv}(s)=\frac{\hat{i}_{bat}}{\hat{v}_{bat}}=-\frac{sC_{o\_cbb}^{\ 2}(2D-1)}{1+(sC_{o\_cbb}L_{cbb})^2} \quad (16)$$

$$G_{ii}(s)=\frac{\hat{i}_{bat}}{\hat{i}_{bus}}=\frac{(1-C_{o\_cbb})}{1+(sC_{o\_cbb}L_{cbb})^2} \quad (17)$$

$$G_{id}(s)=\frac{\hat{i}_{bat}}{\hat{d}}=-\frac{2sC_{o\_cbb}^{\ 2}\bar{V}_{bat}}{1+(sC_{o\_cbb}L_{cbb})^2} \quad (18)$$

$$G_{c1}(s)=\frac{E_{av}}{\Delta V}=\frac{\varphi_vK_{av}R_{av}(sK_{VC}^{P}+K_{VC}^{I})}{s^2J_vR_{av}+sD_vR_{av}+s(\varphi_vK_{av})^2} \quad (19)$$

$$G_{c2}(s)=\frac{I_{bat}^{*}}{E_{av}-V_{bus}}=\frac{V_{bus}^{*}}{R_{av}V_{bat}^{*}} \quad (20)$$

$$G_{c3}(s)=\frac{d}{\Delta I_{bat}}=\frac{sK_{CC}^{P}+K_{CC}^{I}}{s} \quad (21)$$

Therefore, $G_m(s)=1$ and using Equations 13-21, we reach Equation 22:

$$G_{vo}(s)=\frac{G_{c1}(s)G_{c2}(s)G_{c3}(s)G_m(s)G_{vd}(s)}{1+G_{c3}(s)G_{id}(s)+G_{c2}(s)G_{c3}(s)G_m(s)G_{vd}(s)} \quad (22)$$

It should be noted that the stability of other DCMG components at the outset has been demonstrated in previous papers; thus, this paper applies the stability analysis to the proposed VDCM unit and the analysis of the other units is omitted. In the following, according to the explanations given, it is clear that by emulation of virtual inertia through the proposed strategy, the VDCM unit is stable and, along with other components, leads to DCMG stability. Bode, Open Loop Step Response, and Root Locus diagrams are shown seperately in Figure 4(a)-4(c), respectively. According to the obtained figures, the effect of J_v and D_v control parameters on VDCM performance can be observed. The value of $J_v = 0.001$ is assumed according to the Bode diagram (Figure 4(a)), but selecting other values for J_v can mimic the high inertia in the system, which causes the DC bus voltage to return to its reference value over a longer period of time when power imbalance occurs in the DCMG. Also, by selecting $D_v = 0.5$ according to the response to the unit step input (Figure 4(b)), the appropriate response of this parameter to disturbances in the system can be seen because considering higher values for this parameter, the system performance is very slow. Also, the system poles are located to the left of the imaginary axis according to the Root Locus diagram (Figure 4(c)). Thus, we conclude that the proposed VDCM can be used as a suitable option to support DCMG in the event of an error.

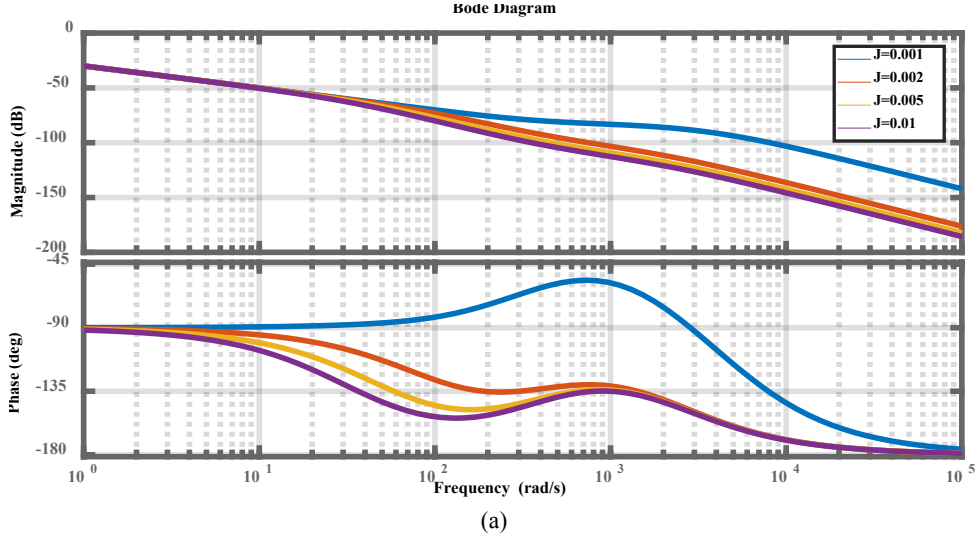

(a)

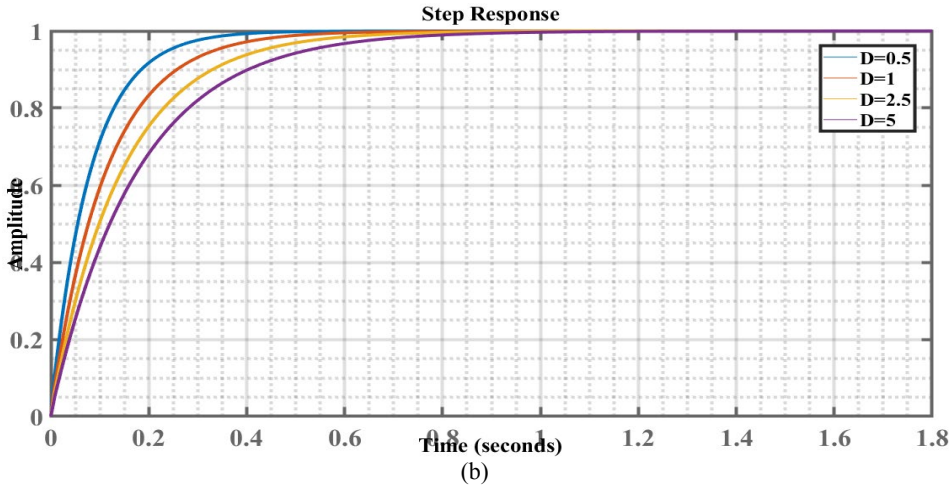

(b)

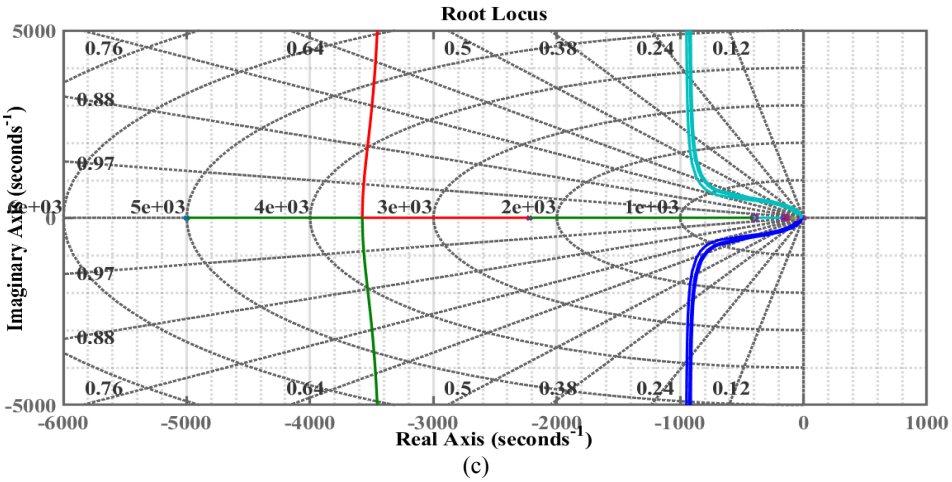

(c)

Figure 4. Stability analysis diagrams of the control system: (a) Bode diagram, (b) Open Loop Step Response diagram, (c) Root Locus diagram

5. SIMULATION RESULTS UNDER DIFFERENT SCENARIOS

Validation and confirmation of the studied DCMG (as shown in Figure 1) has been analyzed according to the proposed control strategy under four scenarios in different operating conditions in Matlab/Simulink environment:

5.1. Virtual inertia control analysis in a system under random load fluctuation

Scenario 1: Evaluate the performance of VDCM in three operating modes: generating, standby and motoring

Figure 5(a) shows the amount of power of the microgrid components, i.e., generating units, VDCM, and energy consumed by the load. In this scenario, the output power of WT, PV, and FC is constant. However, the load increases by amount of 3 KW at 0.6 s and 1.2 s per step such that at the moments between 1.2 s to 1.8 s, microgrid in the amount of 17 KW provides power consumption and at 1.8 s and 2.4 s, as the load added in each step decreases and the load returns to its nominal value. Therefore, the output power of the battery at each stage is proportional to the power required by the microgrid. The proposed control system prevents battery overcurrent at load change moments compared to a conventional VDCM such that in the following, in the load increase and decrease scenario, different parameters of VDCM and DC bus in different functions are discussed, as shown in Figures 5(b), 5(c), and 5(d).

As the load increases, the VDCM performance is shown in Figure 5 from the beginning of the simulation time to 1.8 s. According to Figures 5(a)-5(d), by simulating virtual inertia, it is possible to see the improvement of microgrid performance in simultaneous supply of AC and DC loads. Figure 5(a)-5(d) shows the set of microgrid power and VDCM in microgrid power supply, battery output current, DC link side current, and DC bus voltage, respectively. According to Figures 5(b) and 5(c), which show changes in battery output current and DC link current, VDCM initially generates a mode at 0.6 s in the standby mode and changes to the motoring mode at 1.2 s. As explained in the previous sections, VDCM operation is like a real DC machine. In this way, when the first load is added, i.e., at a moment of 0.6 s, the output currents of the battery and the DC link quickly change from the generating mode to the standby mode. Therefore, according to Figure 5(d), virtual inertia simulation using the proposed scheme compared to VDCM control based on the bidirectional buck-boost converter, the DC bus voltage waveform is placed with much less fluctuation on its reference value. At 1.2 s, when the output current of the battery as well as the current of the DC link change due to the increase in load, the VDCM switches from the standby mode to the motoring mode, which again leads to a slight drop in the DC bus voltage. As shown in Figures 5(b) and 5(c), VDCM provides the required microgrid power.

According to the figure, the microgrid is located at load reduction moments 1.8 s and 2.4 s at which according to the figures, the three motoring, standby, and generating operations occur at the moments before 1.8 s and 2.4 s, respectively. At

1.8 s and 2.4 s, the load is reduced by 3 KW at each stage. The DC bus voltage increases rapidly and by simulating virtual inertia, the bus overvoltage is reduced. Meanwhile, the output currents of the battery and the DC link are also negative due to the change in load and VDCM is switched from the motoring mode to standby and, then, to the generating mode. As a result, VDCM performance is significantly improved.

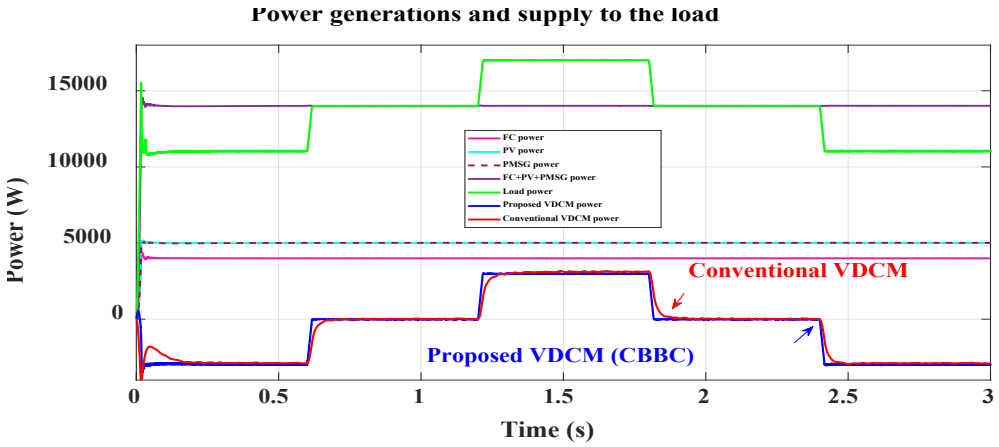

(a) Power waveforms of the DCMG components

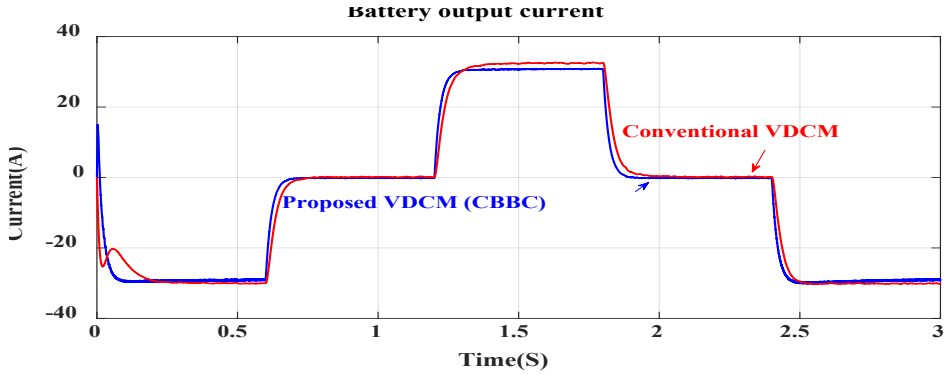

(b) Battery current waveform

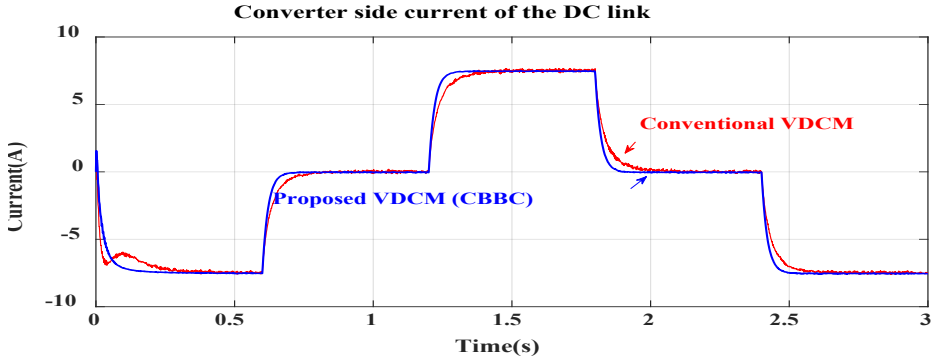

(c) DC link current waveform

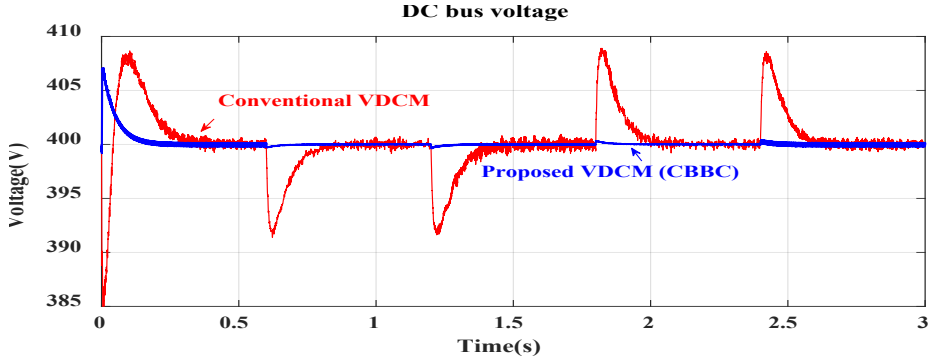

(d) DC bus voltage waveform

Figure 5. The simulation results of the DCMG components power output under constant sources and variable load conditions with 3 KW power in each step, according to the proposed VDCM performance and comparison with the conventional scheme

Scenario 2: Investigation of VDCM performance under load fluctuation changes with increase in 10, 20, and 30 % of rated load

In Scenario 1 in the previous section, the performance of VDCM in different operating modes was examined. Based on the results obtained from the simulation, it is determined that the proposed method has significantly improved the DC bus voltage compared to the conventional VDCM scheme. In addition to improving the bus voltage drop, DCMG's initial transient mode is also completely enhanced. Now, in this section, the tested scenario is related to the entry of random load fluctuations at the moments of 0.4 s, 0.8 s, and 1.2 s. According to Figure 6(a), the load at 0.4 s at 10 % of the nominal load (11 KW + 1.1 KW), 0.8 s at 20 % of the rated load (11 KW + 2.2 KW), and 1.2 s at 30 % of the nominal load (11 KW + 3.3 KW) has been added. Therefore, the microgrid provides a load of 17.6 KW at its maximum capacity at 1.2 s to 1.6 s. In this scenario, VDCM is in two modes of generating and motoring operation. According to Figure 6(b), depending on the needs of the microgrid, the battery is charged at some point (battery output current: negative) and at other times in the discharge mode (battery output current: positive). Also, changes in DC link current can be seen in Figure 6(c). It can be said that the DC link current is in different operating modes (negative or positive) due to the entry and exit random loads to DCMG. On the other hand, the improvement of DC bus voltage changes can also be seen in Figure 6(d).

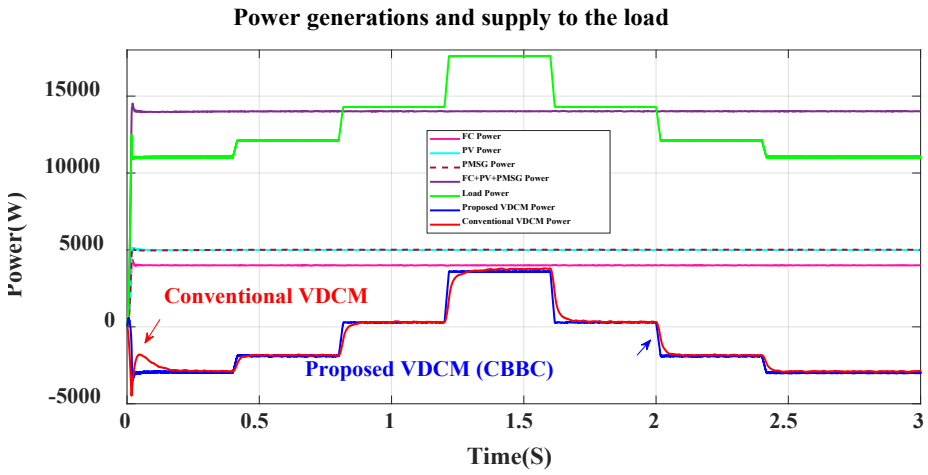

(a) Power waveforms of the DCMG components

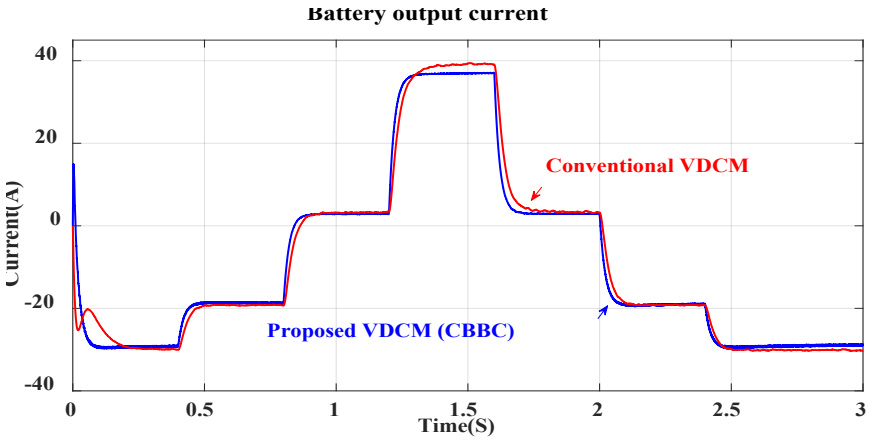

(b) Battery current waveform

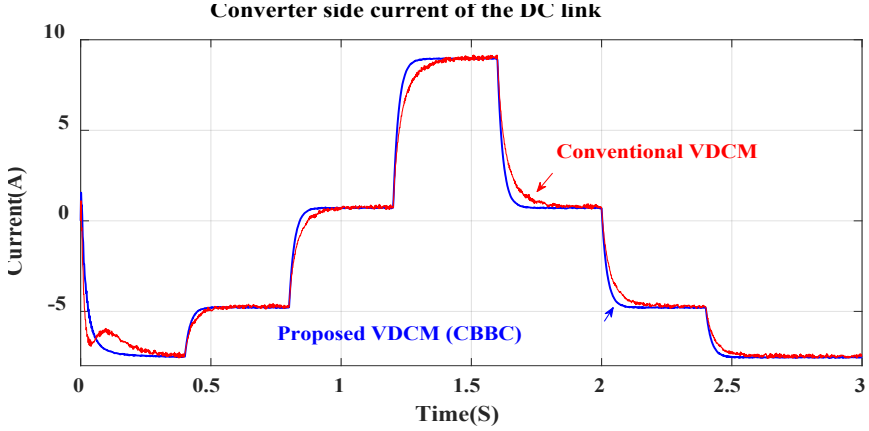

(c) DC link current waveform

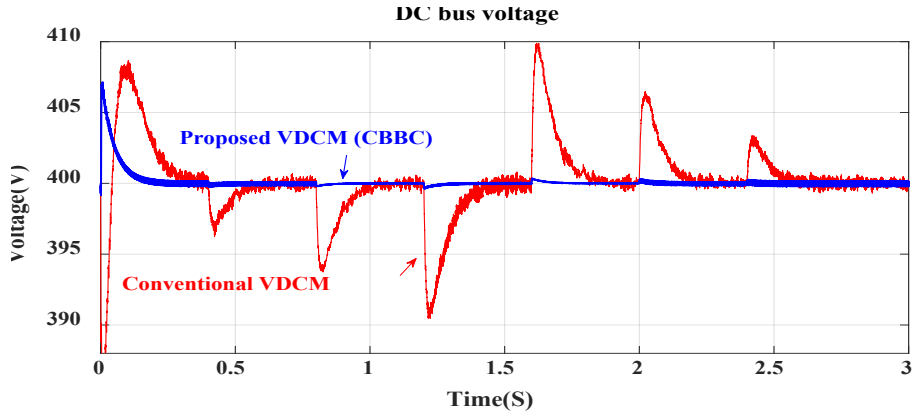

(d) DC bus voltage waveform

Figure 6. The simulation results of the DCMG components power output under constant sources and load fluctuation conditions by increasing 10, 20, and 30 % of nominal load in each step according to the proposed VDCM performance and comparison with the conventional scheme

5.2. Virtual inertia control analysis in a system under the sudden change in generated power and random load fluctuation

Scenario 1: Investigation of VDCM performance under PV rated power changes with random load fluctuations

In this scenario, in addition to the changes in random load fluctuations at 0.4 s, 0.8 s, and 1.2 s, the output power of the PV array according to Figure 7(a) is also equal to 20 % in each step at 0.5 s to 1 s and 2.2 s to 2.7 s decreases. In other words, the power of the microgrid PV array decreases by 1 KW at each time interval and returns to its initial state. Charging and discharging the battery energy storage system can be seen in Figure 7(b) in the conventional scheme compared to the proposed technique. In Figure 7(c), the DC link current changes according to load fluctuations and PV output power. The proposed scheme supports the waves and overvoltages generated as well as transient states and keeps the bus steady for as fewer changes as possible (Figure 7(d)).

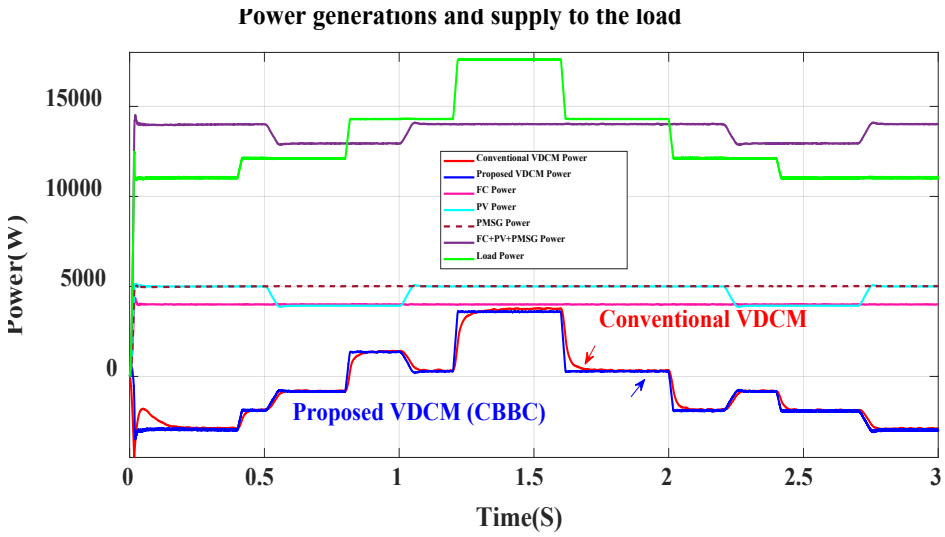

(a) Power waveforms of the DCMG components

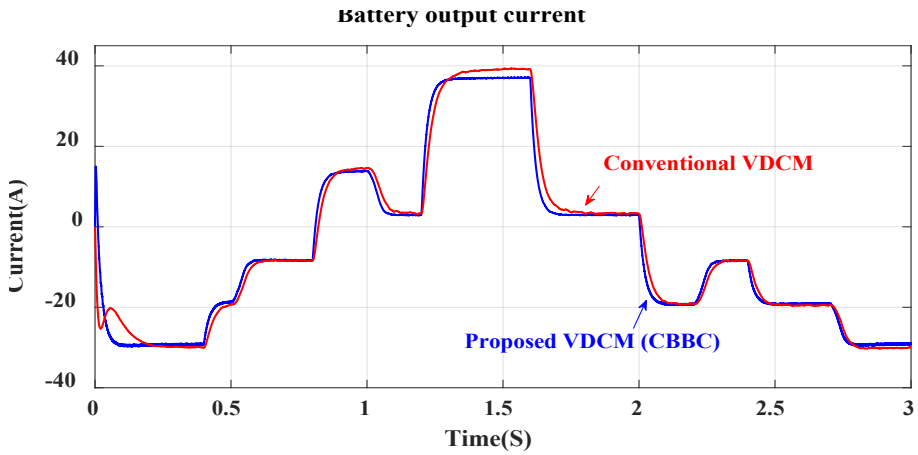

(b) Battery current waveform

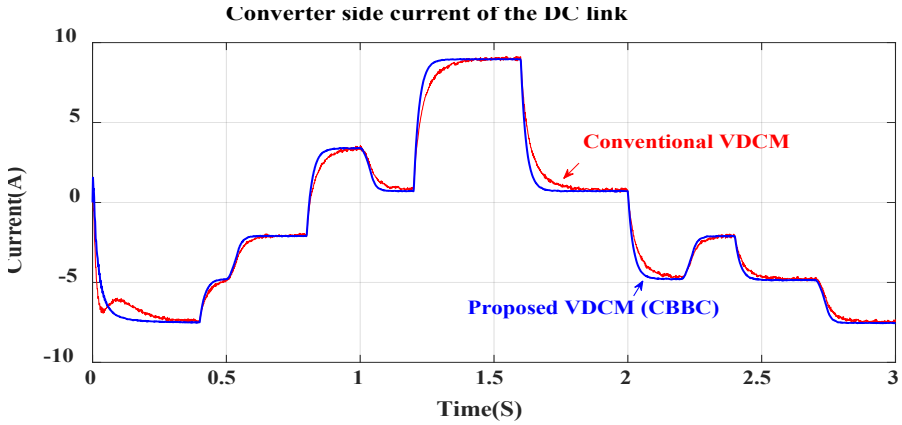

(c) DC link current waveform

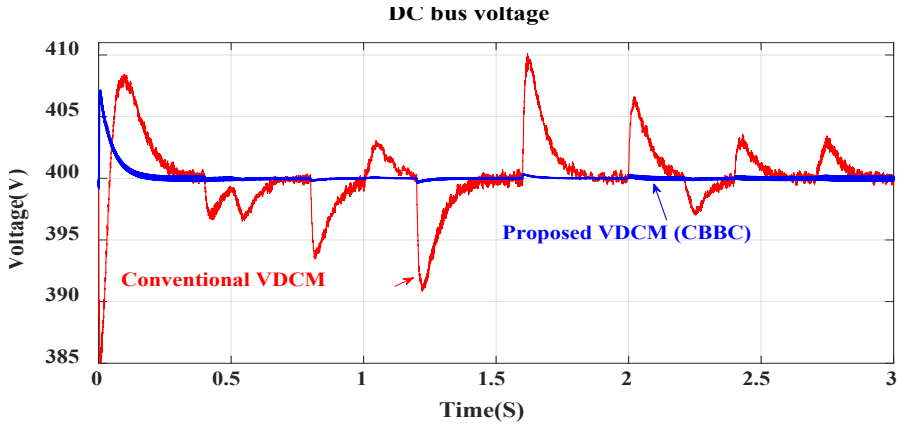

(d) DC bus voltage waveform

Figure 7. The simulation results of the DCMG components power output under 20 % PV source changes in two stages and load fluctuations conditions with increasing 10, 20, and 30 % nominal load in each stage according to the proposed VDCM performance and comparison with the conventional scheme

Scenario 2: Investigation of VDCM performance under rated power changes of PV and PMSG with random load fluctuations

In this scenario, as in the previous scenario, in addition to the changes in random load fluctuations at moments 0.4 s, 0.8 s, and 1.2 s, the output power of the PV arrays and PMSG according to Figure 8(a) as much as 20 % in each step at moments 0.6 s to 1 s and 2.2 s to 2.6 s decreases. In other words, the power of the PV array of the microgrid is reduced by 1 KW in the period of 0.6 s to 1 s and returns to its initial state, and the output power of PMSG decreases by 1 KW in the period of 2.2 s to 2.6 s and returns to the initial state. The transient states of DC bus voltage fluctuations in the conventional VDCM scheme are quite obvious during the changes made in Figure 8(d). However, the proposed scheme supports the waves and overvoltages generated as well as transient states and keeps the bus steady in as little change as possible, and as in Figures 8(b) and 8(c) which represent current waveforms, VDCM proposed is providing the required DCMG power.

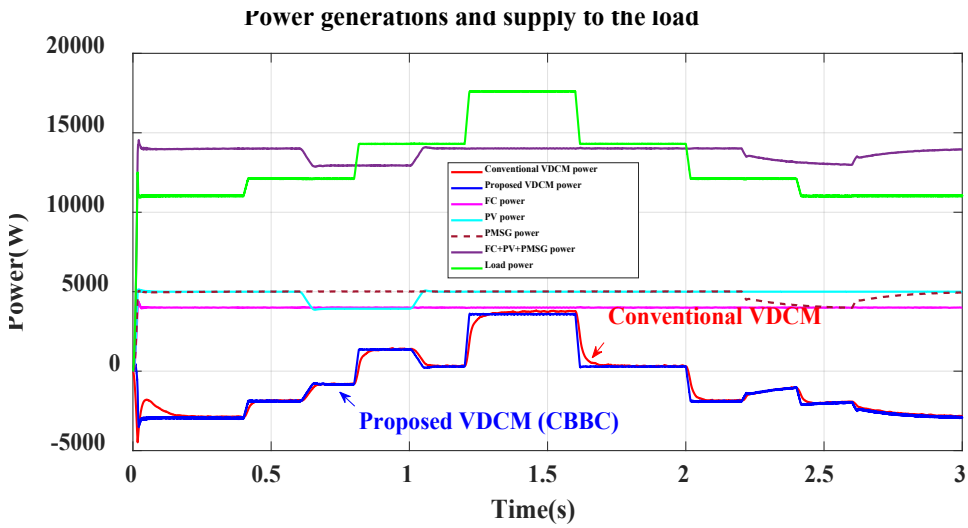

(a) Power waveforms of the DCMG components

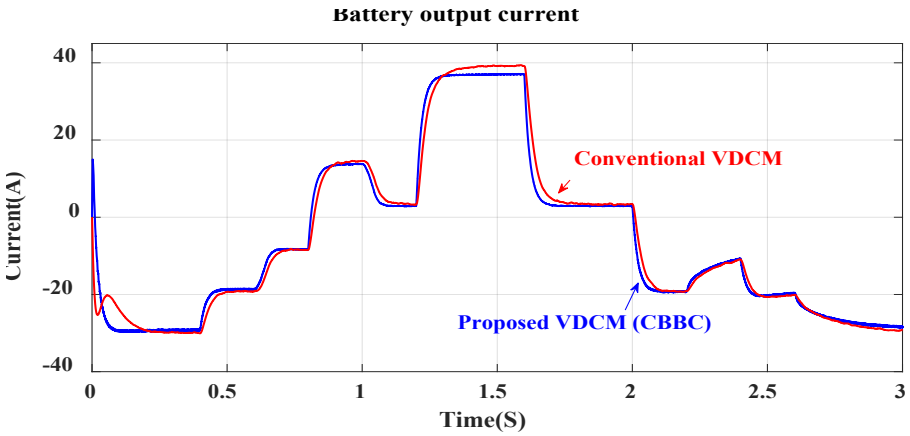

(b) Battery current waveform

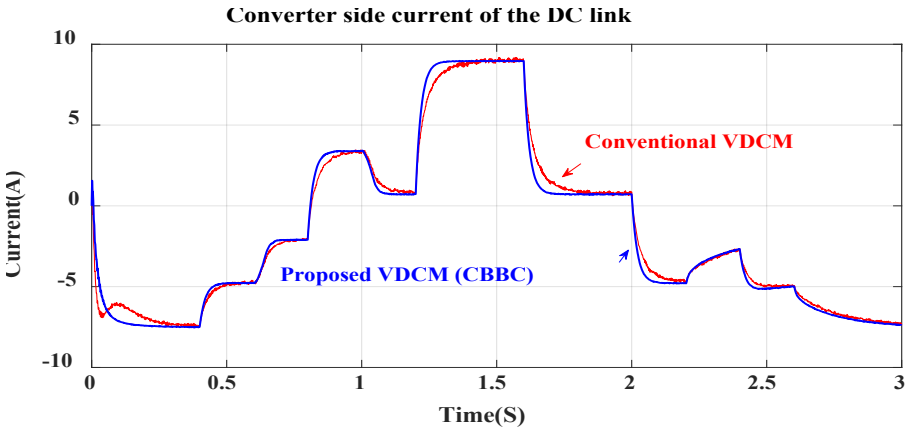

(c) DC link current waveform

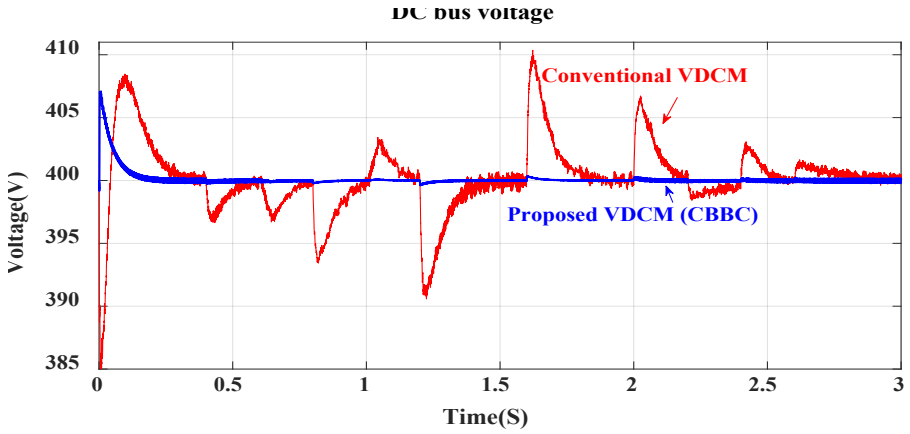

(d) DC bus voltage waveform

Figure 8. The simulation results of the DCMG components under changes of 20 % PV source, 20 % PMSG source, and load fluctuations conditions with increasing 10, 20, and 30 % nominal load in each step according to the proposed VDCM performance and comparison with the conventional scheme

In this section, according to the simulation results obtained during 4 different test scenarios, as can be seen, the performance of the VDCM unit in DCMG is similar in all scenarios. That is, when the consumer unit demand exceeds the output capacity of RESs and FC units, the VDCM unit provides the power required by the consumer and its output specifications are in the motoring mode (discharging). On the other hand, when the consumer demand is less than the production capacity of the microgrid, the output specifications of the VDCM unit are in generating mode (charging) and the extra microgrid power is stored in this unit. Therefore, in the proposed scheme, in order to meet the needs of the consumer during changes, the DC bus voltage is kept constant at its reference value.

6. CONCLUSIONS

Power fluctuations and DC bus voltage drops in DCMGs have become undeniable due to the presence of RESs. Therefore, the trend to use RESs at high power levels along with the implementation of DCMGs was also welcomed. In order to solve this problem, in this paper, a control strategy called VDCM was designed through a proposed converter that enhanced the inertia of the microgrid. DCMG simulations were performed under different scenarios. According to the

simulation results, the virtual inertia control technique implemented on CBBC improved the voltage stability of the 400 V bus and suppressed fluctuations during sudden changes in sources and load consumption. The effects of J_v and D_v were also investigated using the small-signal model CBBC and control system. Therefore, the VDCM controller for the desired converter had a suitable dynamic characteristic. Finally, it can be said that with a suitable VDCM switch between different motoring and generatering modes, the performance of the microgrid has a significant advantage.

7. ACKNOWLEDGEMENT

The authors thank all the personnel of the 7th Iran Wind Energy Conference (IWEC2021) who published this paper at the conference.

NOMENCLATURE

d	Duty cycle (s)
W_r	Kinetic energy stored in the VDCM (j)
W_e	Electrical energy stored in the output capacitor (j)
ω_{rv}	Virtual rotor speed (rad/s)
J_v	Virtual inertia (kg.m^2)
D_v	Virtual damping
R_{av}	Virtual armature resistance (Ω)
L_v	Virtual inductance (H)
T_{emv}	Virtual electromagnetic torque (N.m)
T_{mv}	Virtual mechanical torque (N.m)
P_{emv}	Virtual electromagnetic power (W)
E_{av}	Inductive armature voltage (V)
V^*_{bat}	Battery voltage reference (V)
V^*_{bus}	DC bus voltage reference (V)
I^*_{bat}	Battery current reference (A)
I_{av}	Virtual armature current (A)
C_{dc}	Output capacitor DC link (F)
P^*_{DCMG}	DC microgrid power reference (W)
P^*_{VDCM}	Virtual DC machine power reference (W)
P^*_{PMSG}	Wind turbine power reference (W)
P_{emv}	Virtual electromagnetic power (W)
E_{av}	Inductive armature voltage (V)
V^*_{bat}	Battery voltage reference (V)
V^*_{bus}	DC bus voltage reference (V)
I^*_{bat}	Battery current reference (I)
I_{av}	Virtual armature current (A)
C_{dc}	Output capacitor DC link (F)
P^*_{DCMG}	DC microgrid power reference (W)
P^*_{VDCM}	Virtual DC machine power reference (W)
P^*_{PMSG}	Wind turbine power reference (W)
P_{emv}	Virtual electromagnetic power (W)

REFERENCES

1. Chauhan, A. and Saini, R., "A review on Integrated Renewable Energy System based power generation for stand-alone applications: Configurations, storage options, sizing methodologies and control", ***Renewable and Sustainable Energy Reviews***, Vol. 38, (2014), 99-120. (https://doi.org/10.1016/j.rser.2014.05.079).
2. Ertugrul, N. and Abbott, D., "DC is the Future [Point of view]", ***Proceedings of the IEEE***, Vol. 108, No. 5, (2020), 615-624. (https://doi.org/10.1109/JPROC.2020.2982707).
3. Sun, Y., Zhao, Z., Yang, M., Jia, D., Pei, W. and Xu, B., "Overview of energy storage in renewable energy power fluctuation mitigation", ***CSEE Journal of Power and Energy Systems***, Vol. 6, No. 1, (2019), 160-173. (https://doi.org/10.17775/CSEEJPES.2019.01950).
4. Byrne, R.H., Nguyen, T.A., Copp, D.A., Chalamala, B.R. and Gyuk, I., "Energy management and optimization methods for grid energy storage systems", ***IEEE Access***, Vol. 6, (2017), 13231-13260. (https://doi.org/10.1109/ACCESS.2017.2741578).
5. Dragicevic, T., Vasquez, J.C., Guerrero, J.M. and Skrlec, D., "Advanced LVDC electrical power architectures and microgrids: A step toward a new generation of power distribution networks", ***IEEE Electrification Magazine***, Vol. 2, No. 1, (2014), 54-65. (https://doi.org/10.1109/MELE.2013.2297033).
6. Hammad, E., Farraj, A. and Kundur, D., "On effective virtual inertia of storage-based distributed control for transient stability", ***IEEE Transactions on Smart Grid***, Vol. 10, No. 1, (2017), 327-336. (https://doi.org/10.1109/TSG.2017.2738633).
7. Zhu, X., Xie, Z., Jing, S. and Ren, H., "Distributed virtual inertia control and stability analysis of dc microgrid", ***IET Generation, Transmission & Distribution***, Vol. 12, No. 14, (2018), 3477-3486. (https://doi.org/10.1049/iet-gtd.2017.1520).
8. Tamrakar, U., Shrestha, D., Maharjan, M., Bhattarai, B.P., Hansen, T.M. and Tonkoski, R., "Virtual inertia: Current trends and future directions", ***Applied Sciences***, Vol. 7, No. 7, (2017), 654. (https://doi.org/10.3390/app7070654).
9. Golpîra, H., Atarodi, A., Amini, S., Messina, A.R., Francois, B. and Bevrani, H., "Optimal energy storage system-based virtual inertia placement: A frequency stability point of view", ***IEEE Transactions on Power Systems***, Vol. 35, No. 6, (2020), 4824-4835. (https://doi.org/10.1109/TPWRS.2020.3000324).
10. Wu, D., Tang, F., Dragicevic, T., Guerrero, J.M. and Vasquez, J.C., "Coordinated control based on bus-signaling and virtual inertia for islanded DC microgrids", ***IEEE Transactions on Smart Grid***, Vol. 6, No. 6, (2015), 2627-2638. (https://doi.org/10.1109/TSG.2014.2387357).
11. Yan, X., Congcong, B. and Yuan, F. editors, "Virtual inertia control strategy at energy-storage terminal in DC microgrid", ***2017 IEEE Conference on Energy Internet and Energy System Integration (EI2)***, (2017), 1-5. (https://doi.org/ 10.1109/EI2.2017.8245653).
12. Yi, Z., Zhao, X., Shi, D., Duan, J., Xiang, Y. and Wang, Z., "Accurate power sharing and synthetic inertia control for dc building microgrids with guaranteed performance", ***IEEE Access***, Vol. 7, (2019), 63698-63708.(https://doi.org/10.1109/ACCESS.2019.2915046).
13. Li, Y., He, L., Liu, F., Li, C., Cao, Y. and Shahidehpour, M., "Flexible voltage control strategy considering distributed energy storages for DC distribution network", ***IEEE Transactions on Smart Grid***, Vol. 10, No. 1, (2017), 163-172. (https://doi.org/10.1109/TSG.2017.2734166).
14. Zhi, N., Ding, K., Du, L. and Zhang, H., "An SOC-based virtual DC machine control for distributed storage systems in DC microgrids", ***IEEE Transactions on Energy Conversion***, Vol. 35, No. 3, (2020), 1411-1420. (https://doi.org/10.1109/TEC.2020.2975033).
15. Yang, Y., Li, C., Xu, J., Blaabjerg, F. and Dragičević, T., "Virtual inertia control strategy for improving damping performance of DC microgrid with negative feedback effect", ***IEEE Journal of Emerging and Selected Topics in Power Electronics***, Vol. 9, No. 2, (2020), 1241-1257. (https://doi.org/10.1109/JESTPE.2020.2998812).
16. Guo, L., Zhang, S., Li, X., Li, Y.W., Wang, C. and Feng, Y., "Stability analysis and damping enhancement based on frequency-dependent virtual impedance for DC microgrids", ***IEEE Journal of Emerging and Selected Topics in Power Electronics***, Vol. 5, No. 1, (2016), 338-350. (https://doi.org/10.1109/JESTPE.2016.2598821).
17. Li, C., Li, Y., Cao, Y., Zhu, H., Rehtanz, C. and Häger, U., "Virtual synchronous generator control for damping DC-side resonance of VSC-MTDC system", ***IEEE Journal of Emerging and Selected Topics in Power Electronics***, Vol. 6, No. 3, (2018), 1054-1064. (https://doi.org/10.1109/JESTPE.2018.2827361).
18. Rouzbehi, K., Candela, J.I., Gharehpetian, G.B., Harnefors, L., Luna, A. and Rodriguez, P., "Multiterminal DC grids: Operating analogies to AC power systems", ***Renewable and Sustainable Energy Reviews***, Vol. 70, (2017), 886-895. (https://doi.org/10.1016/j.rser.2016.11.270).
19. Hirase, Y., Sugimoto, K., Sakimoto, K. and Ise, T., "Analysis of resonance in microgrids and effects of system frequency stabilization using a virtual synchronous generator", ***IEEE Journal of Emerging and Selected Topics in Power Electronics***, Vol. 4, No. 4, (2016), 1287-1298. (https://doi.org/10.1109/JESTPE.2016.2581818).
20. Zhu, X., Meng, F., Xie, Z. and Yue, Y., "An inertia and damping control method of DC–DC converter in DC microgrids", ***IEEE Transactions on Energy Conversion***, Vol. 35, No. 2, (2019), 799-807. (https://doi.org/10.1109/TEC.2019.2952717).
21. Lin, G., Zuo, W., Li, Y., Liu, J., Wang, S. and Wang, P., "Comparative analysis on the stability mechanism of droop control and VID control in DC microgrid", ***Chinese Journal of Electrical Engineering***, Vol. 7, No. 1, (2021), 37-46. (https://doi.org/10.23919/CJEE.2021.000003).

22. dos Santos Neto, P.J., dos Santos Barros, T.A., Silveira, J.P.C., Ruppert Filho, E., Vasquez, J.C. and Guerrero, J.M., "Power management strategy based on virtual inertia for DC microgrids", ***IEEE Transactions on Power Electronics***, Vol. 35, No. 11, (2020), 12472-12485. (https://doi.org/10.1109/TPEL.2020.2986283).

23. Samanta, S., Mishra, J.P. and Roy, B.K., "Virtual DC machine: An inertia emulation and control technique for a bidirectional DC–DC converter in a DC microgrid", ***IET Electric Power Applications***, Vol. 12, No. 6, (2018), 874-884. (https://doi.org/10.1049/iet-epa.2017.0770).

24. Chen, X., Pise, A.A. and Batarseh, I., "Magnetics-based efficiency optimization for low power cascaded-buck-boost converter", ***IEEE Transactions on Circuits and Systems I: Regular Papers***, Vol. 67, No. 12, (2020), 5611-5623. (https://doi.org/10.1109/TCSI.2020.2994940).

25. Wang, Z., Chen, B., Zhu, L., Zheng, Y., Guo, J., Chen, D., Ho, M. and Leung, K.N., "A 3.3-MHz fast-response load-dependent-on/off-time buck-boost DC-DC converter with low-noise hybrid full-wave current sensor", ***Microelectronics Journal***, Vol. 74, (2018), 1-12. (https://doi.org/10.1016/j.mejo.2018.01.010)

26. Samanta, S., Mishra, J.P. and Roy, B.K., "Virtual DC machine: An inertia emulation and control technique for a bidirectional DC–DC converter in a DC microgrid", ***IET Electric Power Applications***, Vol. 12, No. 6, (2018), 874-884. (http://doi.org/10.1049/iet-epa.2017.0770).

27. Erickson, R.W. and Maksimović, D., Fundamentals of power electronics, Springer Science & Business Media, New York, (2007). (https://doi.org/10.1007/b100747).